JOURNAL OF SOLID STATE CHEMISTRY 57, 300–313 (1985)

Crystal Structure, Dimensionality, and 4*d* Electron Distribution in $K_{0.30}MoO_3$ and $Rb_{0.30}MoO_3$

M. GHEDIRA,* J. CHENAVAS, AND M. MAREZIO

Laboratoire de Cristallographie, Centre National de la Recherche Scientifique, Laboratoire associé à L'U.S.M.G., 166 X, 38042 Grenoble Cédex, France

AND J. MARCUS

Laboratoire d'Etudes des Propriétés Electroniques des Solides, Centre National de la Recherche Scientifique, Laboratoire associé à l'U.S.M.G., 166 X, 38042 Grenoble Cédex, France

Received July 2, 1984; in revised form September 24, 1984

Single crystals of $K_{0.30}MoO_3$ and $Rb_{0.30}MoO_3$ were synthesized by electrolytic reduction of MoO_3/A_2MoO_4 melts. The crystal structures were refined from X-ray diffraction data (3265 and 1280 independent reflections, respectively). The final R and wR factors were 0.037 and 0.047 for the K bronze and 0.031 and 0.033 for the Rb bronze. The lattice parameters of the body-centered cells used in the present refinements were: $K_{0.30}MoO_3$, a = 16.2311(7), b = 7.5502(4), c = 9.8614(4) Å, β = 94.895(4)°; $Rb_{0.30}MoO_3$, a = 16.361(3), b = 7.555(1), c = 10.094(2) Å, β = 93.87(5)°. The 4*d* electron distribution over the 20 Mo sites [4Mo(1), 8Mo(2), 8Mo(3)] of the unit cell are 10, 45, and 45% for $K_{0.30}MoO_3$ and 14, 43, and 43% for $Rb_{0.30}MoO_3$, respectively. In both cases about 90% of the 4*d* electrons are situated on those sites which contribute to the electrical conductivity. The variations of the lattice parameters versus temperature are reported. The thermal linear-expansion coefficient is highly anisotropic. The structural dimensionality depends upon the sublattice under consideration. The K, Mo, and O sublattices are mono-, two-, and three-dimensional, respectively. The relationship between the structural dimensionality of $K_{0.30}MoO_3$ and the physical properties is discussed.

Introduction

The A_xTO_m bronzes belong to a class of compounds in which A is an alkali metal and T one of the following elements: Ti, V, Nb, Pt, Pd, W, or Mo. They have a variety of crystal structures and consequently a variety of physical properties.

The red and blue potassium bronzes, $K_{0.33}MoO_3$ and $K_{0.30}MoO_3$, were first prepared by Wold *et al.* (*1*). They are not isostructural (*2, 3*) and the former is a semiconductor while the latter exhibits a metal-to-semiconductor phase transition at T_c = 180 K (*4–6*).

As determined by Graham and Wadsley (*3*) the crystal structure of $K_{0.30}MoO_3$ is monoclinic, space group $C2/m$, with 20 formulae per unit cell of dimensions a = 18.25(1), b = 7.560(5), c = 9.885(6) Å, β = 117.5(1)°. The atoms occupy the positions given in Table I. The structure contains

* Permanent address: Faculté des Sciences et Techniques, Monastir, Tunisie.

0022-4596/85 $3.00

TABLE I

POSITIONAL AND THERMAL PARAMETERS[a]

	X	Y	Z	U_{11}	U_{22}	U_{33}	U_{12}	U_{13}	U_{23}
K(1)	0	½	½	.0357(10)	.0262(9)	.0492(12)	0	−.2007(9)	0
Rb(1)	0	½	½	.0248(7)	.0177(6)	.0406(8)	0	−.0094(6)	0
K(2)	.81198(7)	0	.5314(1)	.0254(5)	.0217(5)	.0207(5)	0	.0072(4)	0
Rb(2)	.81592(6)	0	.5326(1)	.0202(4)	.0145(4)	.0195(4)	0	.0050(3)	0
Mo(1)	.22593(2)	0	.05216(3)	.0072(1)	.0078(1)	.0101(2)	0	.0017(1)	0
	.22380(5)	0	.04931(8)	.0073(3)	.0038(3)	.0124(3)	0	.0013(2)	0
Mo(2)	.42052(2)	.24475(3)	.37779(2)	.0078(1)	.0071(1)	.0081(1)	.0001(1)	.0024(1)	−.0003(1)
	.42244(3)	.24415(7)	.38128(5)	.0080(2)	.0028(2)	.0097(2)	.0002(2)	.0016(2)	−.0004(2)
Mo(3)	.13856(1)	.24993(3)	.79216(2)	.0089(1)	.0071(1)	.0083(1)	.0003(1)	.0034(1)	.0005(1)
	.13968(3)	.25002(7)	.79606(5)	.0086(2)	.0029(2)	.0101(2)	.0003(2)	.0027(1)	.0004(2)
O(1)	¼	¼	¾	.011(1)	.013(1)	.022(2)	.001(1)	.008(1)	.005(1)
	¼	¼	¾	.011(2)	.004(2)	.025(3)	.001(2)	.008(2)	.002(3)
O(2)	.2497(2)	0	.2225(3)	.017(1)	.022(2)	.014(1)	0	.003(1)	0
	.2493(4)	0	.2167(7)	.016(3)	.020(3)	.013(3)	0	.001(3)	0
O(3)	.3182(2)	0	.9830(3)	.011(1)	.019(1)	.016(1)	0	.007(1)	0
	.3156(4)	0	.9799(7)	.011(3)	.018(3)	.015(3)	0	.002(2)	0
O(4)	.4199(2)	0	.4087(3)	.014(1)	.008(1)	.016(1)	0	.002(1)	0
	.4222(4)	0	.4139(7)	.014(3)	.008(3)	.014(3)	0	.001(2)	0
O(5)	.9118(2)	0	.9046(3)	.008(1)	.009(1)	.017(1)	0	.002(1)	0
	.9126(4)	0	.9035(7)	.011(3)	.001(2)	.022(3)	0	.002(2)	0
O(6)	.1554(2)	0	.8425(3)	.011(1)	.007(1)	.012(1)	0	.000(1)	0
	.1564(3)	0	.8459(6)	.004(2)	.002(2)	.014(3)	0	.003(2)	0
O(7)	.6411(2)	0	.3102(3)	.017(1)	.009(1)	.018(1)	0	.009(1)	0
	.6423(4)	0	.3142(7)	.015(3)	.003(2)	.021(3)	0	.007(3)	0
O(8)	.3988(2)	.2448(3)	.2085(2)	.019(1)	.019(1)	.013(1)	−.002(1)	−.001(1)	−.001(1)
	.4016(3)	.2397(7)	.2153(5)	.020(2)	.014(2)	.014(2)	.004(2)	−.001(2)	.000(3)
O(9)	.1854(1)	.2432(3)	.0241(2)	.008(1)	.009(1)	.012(1)	.000(1)	.003(1)	−.001(1)
	.1836(3)	.2433(6)	.0223(4)	.010(2)	.001(2)	.017(2)	.002(2)	.001(1)	.000(2)
O(10)	.0884(2)	.2192(3)	.6376(2)	.019(1)	.018(1)	.012(1)	−.002(1)	.000(1)	.001(1)
	.897(3)	.2196(6)	.6466(5)	.017(2)	.010(2)	.015(2)	−.002(2)	.001(2)	−.002(2)
O(11)	.0377(1)	.2463(3)	.8916(2)	.009(1)	.013(1)	.009(1)	.001(1)	.003(1)	.001(1)
	.0382(2)	.2443(6)	.8940(3)	.008(1)	.008(1)	.010(2)	−0.01(2)	.004(1)	.000(2)

[a] For each position the first line gives the parameters of $K_{0.30}MoO_3$ while the second line gives those of $Rb_{0.30}MoO_3$.

rigid units comprised of 10 distorted MoO_6 octahedra. The arrangement of one unit is shown in Fig. 1. The units are linked together via corner sharing along two directions, **b** and [102], so as to form one-unit wide slabs (shown in Fig. 2). The slabs are held together by K–O bonds. It is interesting to note that the linking between units is made by the Mo(2) and Mo(3) octahedra, while the Mo(1) octahedra share their edges and corners only with the Mo(2) and Mo(3) octahedra of the same unit. With such an arrangement $K_{0.30}MoO_3$ has been considered to be a two-dimensional compound as far as the Mo sublattice is concerned.

Brusetti *et al.* (*7*) showed that for $T > T_c$ the electrical conductivity, as measured from single-crystal samples, has a very anisotropic behavior. For instance, at room temperature the conductivity along the **b** axis is about 10 times that measured along the [102] direction, and about 100 times that along the direction perpendicular to the slabs of MoO_6 octahedra. Furthermore,

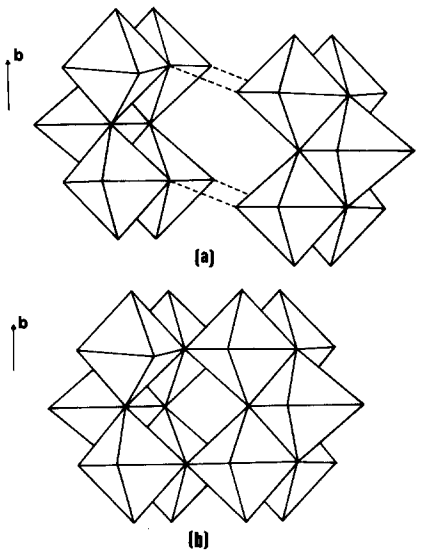

FIG. 1. (a) Two five-octahedron units joining together so as to form (b) a ten-octahedron unit.

Brusetti *et al.* (*7*) showed that the way the electrical conductivity varies with temperature for $T > T_c$, also depends upon the crystallographic direction. It increases with decreasing temperature along the **b** axis while it is nearly temperature independent along the [102] direction. From optical reflectivity measurements carried out on single crystals, Travaglini *et al.* (*8*) deduced that $K_{0.30}MoO_3$ is a quasi-1-D conductor and that the 180 K transition is of Peierls type. These results were later confirmed by Raman scattering measurements (*9*). Recently, Dumas *et al.* (*10*) reported that below the transition the electrical conductivity exhibits a nonohmic behavior when the applied field is greater than a small threshold field ($E_T \sim 130$ mV/cm).

Pouget *et al.* (*11*) reported that mono-

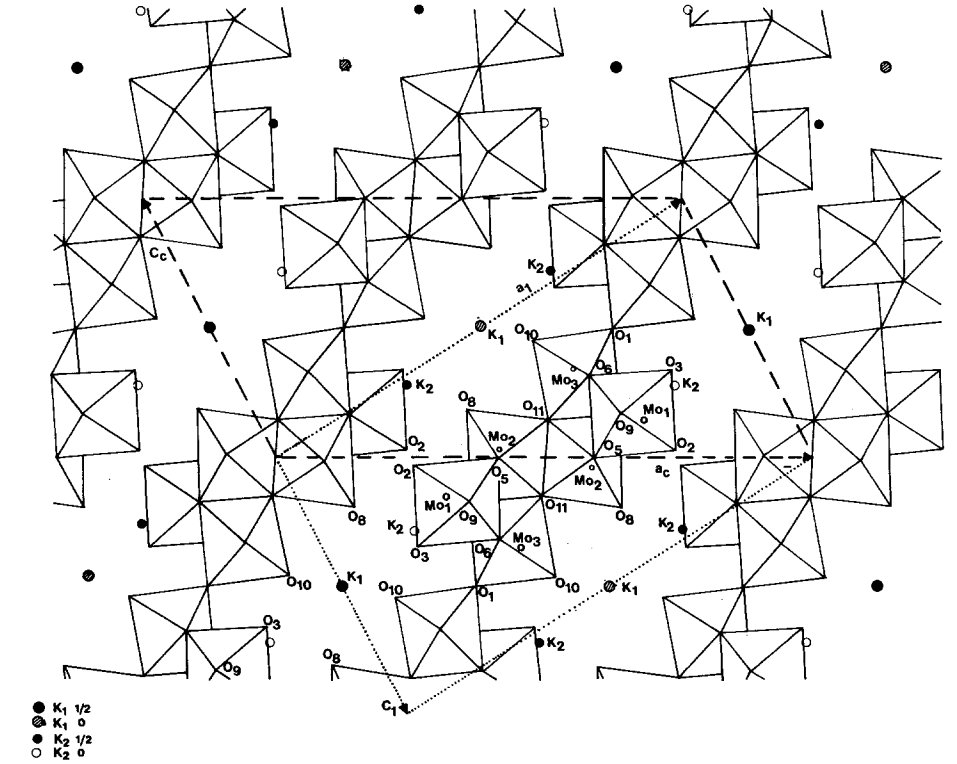

FIG. 2. Projection on the (010) plane, showing the octahedral slabs. The C- and I-centered unit cells are both indicated. The oxygen octahedra are outlined. Each ten-octahedron unit is represented by a group of six octahedra as four sets of two octahedra are coincident in this projection.

chromatic X-ray Laue and Weissenberg photographs taken above the transition, contained diffuse streaks normal to the **b*** reciprocal direction. These diffuse streaks looked like flattened cigars pointed in the $2\mathbf{a}^*-\mathbf{c}^*$ reciprocal direction and were situated at $\pm q_b\mathbf{b}^*$ from planes with odd k indices. Since the q_b value was 0.28, the diffuse streaks were incommensurate with the crystal lattice. Below the transition well-defined superstructure reflections were observed. The wave vector of these satellites was found to be $\mathbf{q} = 0\mathbf{a}^* + q_b\mathbf{b}^* + 0.5\mathbf{c}^*$ with q_b slightly greater than 0.25, still incommensurate with the crystal lattice. The satellites related to Bragg spots with k odd, were considered to be a condensation of the high-temperature diffuse streaks. Chen *et al.* (*12*) confirmed the appearance of the superstructure spots below the transition by electron diffraction studies. These authors reported that the superstructure stable below the 180 K transition is very sensitive to electron-beam irradiation. Very recently Fleming and Schneemeyer (*13*) showed that $K_{0.30}MoO_3$ underwent an incommensurate-to-commensurate transition at 110 K where the **q** vector became ($0a^*$, $0.25b^*$, $0.5c^*$). By Raman scattering studies Dierker *et al.* (*14*) confirmed the existence of the 110 K transition and showed that this transition can be suppressed by small amounts of impurities.

In order to relate the crystal structure and its dimensionality to the physical properties, we undertook a very precise structural refinement of $K_{0.30}MoO_3$ at room temperature. Since the Rb counterpart has similar physical properties (*15*), we carried out the structural refinement of $Rb_{0.30}MoO_3$ as well.

Experimental

(a) Preparation. Single crystals of the blue bronzes were grown by electrolytic reduction of MoO_3/A_2MoO_4 melts having a 3.35/1 mole ratio. The starting materials were melted in a Pt crucible at 565°C by using a vertical tube furnace. A current of 40 mA was maintained through the melt during 3 to 16 hr by means of two electrodes. The anode and the cathode were a 1-cm^2 sheet and a wire, respectively. Easily cleavable single crystals with average dimensions of $5 \times 2 \times 1$ mm were obtained for $K_{0.30}MoO_3$, the **b** and the [102] directions lying along the largest and the medium dimensions, respectively. The single crystals of $Rb_{0.30}MoO_3$ were of smaller dimensions.

(b) Intensity data collections. From fractured single crystals of $K_{0.30}MoO_3$ and $Rb_{0.30}MoO_3$, two irregularly shaped samples suitable for X-ray diffraction experiments were isolated, the largest dimensions being in both cases less than 0.12 mm. Precession photographs taken with filtered Mo$K\alpha$ radiation were indexed on the unit cell proposed by Graham and Wadsley (*3*). The $C2/m$ space group was confirmed and preliminary lattice parameters were obtained. For $K_{0.30}MoO_3$ long-exposure ($\simeq$250 hr) precession photographs of the lattice plane containing the b^* and $2a^*-c^*$ directions and of that containing the b^* and c^* directions, did not reveal any trace of the diffuse streaks observed by Pouget *et al.* (*11*). Streaks should have appeared on the first-type photographs, while extra spots should have appeared on the second type. These experiments were carried out by the use of an X-ray generator equipped with filtered Mo$K\alpha$ radiation and operated at 1.5 kW. The same single crystals of $K_{0.30}MoO_3$ and $Rb_{0.30}MoO_3$ were mounted on a Philips four-circle diffractometer equipped with a graphite monochromator and Mo$K\alpha$ radiation. Both data collections were carried out by the use of a body-centered I-unit cell related to the C-centered unit cell of Graham and Wadsley (*3*) by the matrix

$$\begin{pmatrix} a \\ b \\ c \end{pmatrix}_I = \begin{pmatrix} 10\bar{1} \\ 0\bar{1}0 \\ 00\bar{1} \end{pmatrix} \begin{pmatrix} a \\ b \\ c \end{pmatrix}_C$$

The I-cell has the same volume as the C-cell, but the β_I angle, being closer to 90°, facilitates the description of the structure. Note, for example, that the $(201)_C$ plane of the Graham and Wadsley lattice, which is parallel to the octrahedral slabs, becomes the $(101)_I$ plane of the body-centered lattice. The intensities of all reflections with $\theta \leq 45°$ and $h \geq 0$ were measured by using the ω-scan mode ($\Delta\omega = 1.6 + 0.15$ tn θ). The background was measured on each side of the peak and in order to have a better count statistics for weak reflections the multiscan technique was used. Those reflections for which the integrated intensity was less than twice the background were considered as unobserved. The Lorentz and polarization corrections were applied in order to obtain the structure factors. Due to the dimensions of the sample, the absorption correction was not applied. The μR value was in any direction less than 0.35 for both compounds. After averaging symmetry-related reflections, 3265 and 1280 independent structure factors were obtained for $K_{0.30}MoO_3$ and $Rb_{0.30}MoO_3$, respectively. The significantly smaller number of reflections for the Rb bronze was due to the size of single crystals available for this compound. The largest single crystals of the Rb bronze were about one-third in volume the average crystals of the K bronze.

(c) Lattice parameters. The lattice parameters were determined by using the single crystals mounted on the Philips diffractometer for the intensity data collection. The θ angle of 27 independent reflections with α_1 and α_2 fully separated, were measured. the zero of the θ circle was obtained by measuring the θ and $-\theta$ value for each reflection. The least-squares refinement yielded the following values

$K_{0.30}MoO_3$:

$a = 16.2311(7)$, $b = 7.5502(4)$,
$c = 9.8614(4)$ Å, $\beta = 94.895(4)°$

$Rb_{0.30}MoO_3$:

$a = 16.361(3)$, $b = 7.555(1)$,
$c = 10.094(2)$ Å, $\beta = 93.87(5)°$

The lattice parameters as a function of temperature from 110 K to room temperature were determined for the K bronze. The low temperatures were obtained by blowing nitrogen gas at controlled temperatures over the crystal. The same 27 θ angles were measured every 10 K. The values of the lattice parameters, the unit cell volume, the **a–c** vector and the $d_{[101]_I}$ lattice spacing as function of temperature are reported in Fig. 3.

(d) Structural refinements. During the first stage of refinement the Nonius-Enraf SDP system program was used. The *f*-curves for neutral atoms and the coefficients of the anomalous dispersion correction for K and Mo, were taken from the International Tables for X-ray crystallography. The weighting scheme ($w = 1/\sigma(F^2)$ with a zero fudge factor) was that of the SDP system.

The starting values for the positional and isotropic thermal parameters were those of Graham and Wadsley (*3*). The positional parameters were transformed for the *I2/m* space group. After convergence was attained it was noticed that the strong reflections occurring at low θ angle, were affected by extinction. The final stages of refinement were carried out by the use of the Linex program. Several cycles, during which one scale factor, 34 positional parameters, 78 anisotropic thermal parameters, and one isotropic extinction coefficient were varied, yielded $R(F) = 0.037$ and $wR(F) = 0.047$. The occupancy parameters of the K(1) and K(2) sites were also varied, but since their values remained close to unity within their respective stan-

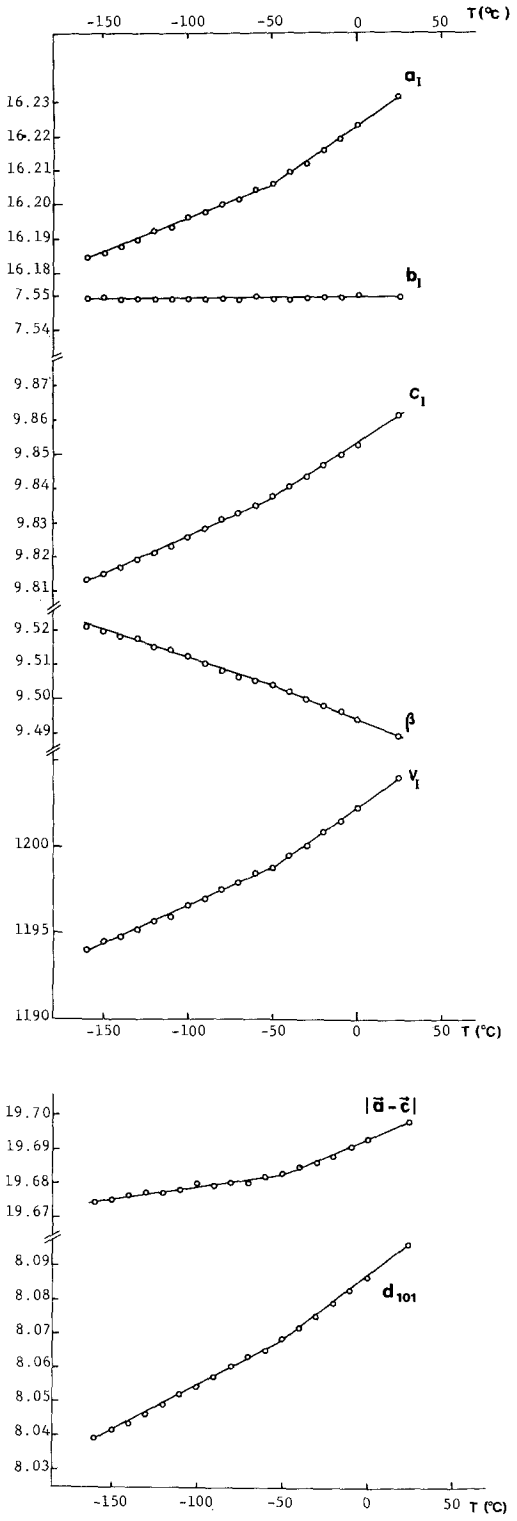

FIG. 3. Lattice parameters versus temperature. The variations of $|\mathbf{a}-\mathbf{c}|_l$ and d_{101} are also shown. The former runs along the octahedral slabs perpendicular to the b axis while the latter runs perpendicularly to the octahedral slabs.

dard deviations, they were kept constant in the final cycle. This indicated that the stoichiometry of the K bronze crystal was indeed $K_{0.30}MoO_3$.

The same procedure was applied to the refinement of the Rb bronze; the starting values were those obtained for the K bronze. The last cycle yielded $R(F) = 0.031$ and $wR(F) = 0.033$. Although the R factor of the Rb bronze are smaller than those of the K bronze, the standard deviations of the former compound are about twice as large the corresponding values of the latter. This is due to the number of reflections used in the structural refinements of the two compounds: 1280 for the Rb bronze and 3265 for the K bronze.

It must be pointed out that the structural refinements were carried out without taking into consideration the diffuse scattering streaks observed by Pouget *et al.* (*11*). Their existence is indicative of some structural disorder–order problem in $K_{0.30}MoO_3$ and $Rb_{0.30}MoO_3$. Since these streaks are very weak, their exclusion should not have any significance on the results presented and discussed herein.

The final positional and thermal parameters are reported in Table I. The interatomic distances together with the corresponding Zachariasen bond strengths (*16*) are listed in Table II while the thermal data are reported in Table III.

Discussion

(1) $K_{0.30}MoO_3$

(a) The interatomic distances and the structural distortion. The distance between two bonded Mo cations occupying two

edge-sharing oxygen octahedra, is about 2.7 Å if the Mo cations form a single bond and 2.5 Å if they form a double bond. In the structure of $K_{0.30}MoO_3$ the shortest Mo–Mo separation across a shared edge is 3.181 Å while the separations of other pairs are even longer. This is illustrated in Fig. 4. Therefore, there are no metal–metal bonds in the room-temperature structure of $K_{0.30}MoO_3$. Because of the large Mo displacements from the octahedral centers, the Mo–O distances vary over a very large range (1.677–2.348). The average Mo–O distances are: Mo(1)–O = 1.983 Å, Mo(2)–O = 1.960 Å, and Mo(3)–O = 1.960 Å, which give 1.964 Å as the overall average. This value is in good agreement with those found in other oxides where the oxidation state of the Mo atoms is between 5 and 6. For instance, in the recently refined $K_{0.9}Mo_6O_{17}$ Vincent *et al.* (*17*) found 1.942 Å for the average octahedral Mo–O distance. The average Mo valence in $K_{0.9}Mo_6O_{17}$ is 5.52 as against 5.70 in the present compound.

The Mo(1) cations are so displaced from the octahedral center that its coordination should be considered as 4 + 2 with the four closest oxygen neighbors forming a distorted tetrahedron. Octahedral distortions

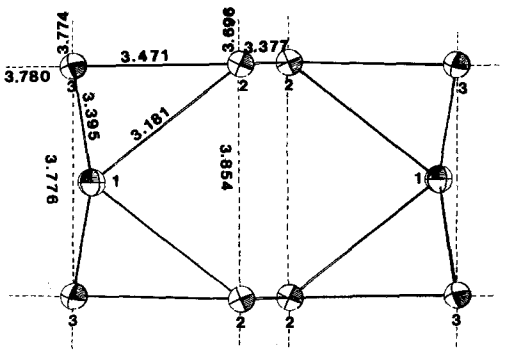

FIG. 4. Mo-sublattice in $K_{0.30}MoO_3$. The Mo–Mo distances inside a ten-octahedron unit and between units are given. The different Mo sites are indicated by arabic numbers. The solid and dotted lines correspond to edge and corner sharing, respectively.

can be characterized by the standard deviation calculated for the six Mo–O distances and/or by that calculated for the 12 O–O distances. The former which gives information on the distortion due to cation displacements, and the latter which gives information on the octahedral shape are not independent; a displaced cation causes an unbalance in the electrostatic charge and consequently the anions move from their positions in order to reestablish the balance. It can be seen from Table II that the distortion due to displacements is much larger for Mo(1) (0.269 Å) than for Mo(2) and Mo(3) (0.214 and 0.218 Å, respectively). The distortions of the Mo(1) and Mo(2) octahedra, as calculated from the O–O distances (0.135 and 0.139 Å, respectively), are larger than that of the Mo(3) octahedron (0.114 Å). These differences are mainly due to the number of edges shared by each octahedron; that around Mo(1) share four of its edges with the adjacent octahedra while those around Mo(2) and Mo(3) share three and two edges, respectively.

The oxygen polyhedron around the K(1) cation is a cube with two opposite faces capped with an additional oxygen, O(3), while that around the K(2) cation is a trigonal prism with one of the square faces capped with an additional oxygen, O(2). The coordination numbers are 10 and 7, respectively. The K(1)–O distances vary over a large range (2.839 to 3.304 Å) while those corresponding to K(2) are closer to the average value; they vary from 2.703 to 2.932 Å. The monocapped trigonal prisms and the bicapped cubes form infinite edge-sharing chains parallel to the *b* axis, as shown in Fig. 5. It deserves attention that the K polyhedra forming the chains, share only corners with the Mo-octahedra forming the slabs. Moreover, the infinite K polyhedra chains are isolated as they do not share any oxygen atom with adjacent K chains.

As can be seen from the interatomic distances, the coordination polyhedra around K(1) are too large for the size of the K^{1+} cations. On the contrary, those around K(2) have the appropriate size. The average K(2)–O distance is 2.854 Å, which agrees well with the value of 2.84 deduced from

TABLE II

INTERATOMIC DISTANCES (Å) AND BOND STRENGTHS

	$K_{0.30}MoO_3$	s	$Rb_{0.30}MoO_3$	s
(1) Octahedron Mo(1)				
–O(2)	1.690(3)	1.892	1.714(7)	1.752
–O(3)	1.698(3)	1.844	1.700(7)	1.832
–O(5)	2.310(3)	0.262	2.313(6)	0.260
–O(6)	2.276(3)	0.292	2.262(6)	0.306
–O(9) × 2	1.962(2)	0.795	1.964(4)	0.790
Average	1.983		1.986	
Distortion coefficient	0.269		0.261	
Σs		5.880		5.730
O(9)–O(5) × 2	2.557(3)		2.564(6)	
–O(2) × 2	2.817(3)		2.847(6)	
–O(3) × 2	2.887(3)		2.889(7)	
–O(6) × 2	2.582(3)		2.575(6)	
O(2)–O(3)	2.694(4)		2.691(8)	
–O(5)	2.806(4)		2.840(8)	
O(6)–O(3)	2.878(4)		2.853(8)	
–O(5)	2.805(4)		2.837(8)	
Average	2.739		2.748	
Distortion coefficient	0.135		0.141	
(2) Octahedron Mo(2)				
–O(8)	1.677(2)	1.972	1.686(5)	1.916
–O(11)	1.896(2)	0.981	1.892(4)	0.994
–O(11)	2.319(2)	0.255	2.318(4)	0.256
–O(4)	1.873(2)	1.056	1.874(2)	1.052
–O(5)	1.952(1)	0.821	1.954(2)	0.815
–O(9)	2.045(2)	0.610	2.049(4)	0.602
Average	1.960		1.962	
Distortion coefficient	0.214		0.211	
Σs		5.695		5.635
O(5)–O(11)	2.774(3)		2.769(6)	
–O(11)	2.809(3)		2.830(7)	
–O(9)	2.557(3)		2.564(6)	
–O(8)	2.726(3)		2.735(7)	
O(4)–O(11)	2.722(3)		2.724(6)	
–O(11)	2.791(3)		2.782(6)	
–O(9)	2.704(3)		2.707(6)	
–O(8)	2.706(3)		2.704(7)	
O(8)–O(11)	2.766(3)		2.777(6)	
–O(9)	3.074(3)		3.080(6)	
O(11)–O(11)	2.533(4)		2.551(8)	
–O(9)	2.631(3)		2.694(5)	
Average	2.733		2.743	
Distortion coefficient	0.139		0.135	
(3) Octahedron Mo(3)				
–O(10)	1.682(2)	1.941	1.683(5)	1.934
–O(9)	2.348(2)	0.232	2.347(4)	0.233
–O(1)	1.890(0)	1.000	2.894(1)	0.987
–O(7)	1.897(0)	0.978	1.898(1)	0.975
–O(6)	1.964(1)	0.790	1.989(2)	0.729
–O(11)	1.979(2)	0.753	1.969(4)	0.777
Average	1.960		1.963	
Distortion coefficient	0.218		0.217	
Σs		5.694		5.635

TABLE II—*Continued*

	$K_{0.30}MoO_3$ s	$Rb_{0.30}MoO_3$ s
O(6)–O(1)	2.644(2)	2.655(4)
–O(10)	2.762(3)	2.774(7)
–O(11)	2.738(3)	2.741(6)
–O(9)	2.582(3)	2.575(6)
O(7)–O(1)	2.687(2)	2.693(5)
–O(10)	2.807(3)	2.810(6)
–O(11)	2.714(3)	2.731(7)
–O(9)	2.909(3)	2.905(7)
O(1)–O(9)	2.982(2)	3.022(4)
–O(11)	2.769(2)	2.767(5)
O(10)–O(9)	2.710(3)	2.694(6)
–O(11)	2.631(3)	2.631(5)
Average	2.745	2.750
Distortion coefficient	0.144	0.122
(4) Polyhedron K(1)		Polyhedron Rb(1)
–O(8) × 4	3.304(2)	3.325(5)
–O(10) × 4	2.839(2)	2.923(5)
–O(3) × 2	2.941(3)	3.009(7)
Average	3.045	3.101
O(8)–O(10) × 4	3.225(4)	3.213(7)
–O(10) × 4	3.447(3)	3.680(7)
–O(8) × 2	3.697(5)	3.617(9)
O(10)–O(10) × 2	4.240(4)	4.235(9)
O(3)–O(8) × 4	3.094(3)	3.231(7)
–O(10) × 4	2.918(3)	2.966(7)
(5) Polyhedron K(2)		Polyhedron Rb(2)
–O(8) × 2	2.885(2)	2.983(5)
–O(9) × 2	2.822(2)	2.903(4)
–O(10) × 2	2.932(3)	2.964(5)
–O(2)	2.703(3)	2.811(7)
Average	2.854	2.929
O(9)–O(8) × 2	3.772(3)	3.949(6)
–O(10) × 2	4.136(3)	4.195(6)
O(8)–O(10) × 2	3.447(3)	3.680(7)
–O(8)	3.854(5)	3.938(9)
O(9)–O(9)	3.878(4)	3.880(8)
O(10)–O(10)	3.311(5)	3.316(9)
O(2)–O(8) × 2	3.203(4)	3.267(6)
–O(9) × 2	3.267(3)	3.394(7)

(6) Mo–Mo distances[a]	$K_{0.30}MoO_3$	$Rb_{0.30}MoO_3$
Inside a 10-octahedron unit		
Mo(1)–Mo(2) a	3.181	3.190
Mo(1)–Mo(3) a	3.395	3.394
Mo(2)–Mo(2) a	3.377	3.371
Mo(2)–Mo(2) b	3.854	3.866
Mo(2)–Mo(3) a	3.471	3.477
Mo(3)–Mo(3) b	3.776	3.778
Between 10-octahedron units		
Mo(2)–Mo(2) b	3.696	3.689
Mo(3)–Mo(3) b	3.774	3.777
Mo(3)–Mo(3) b	3.780	3.788

[a] *a* and *b* indicate across a shared edge and a shared corner, respectively.

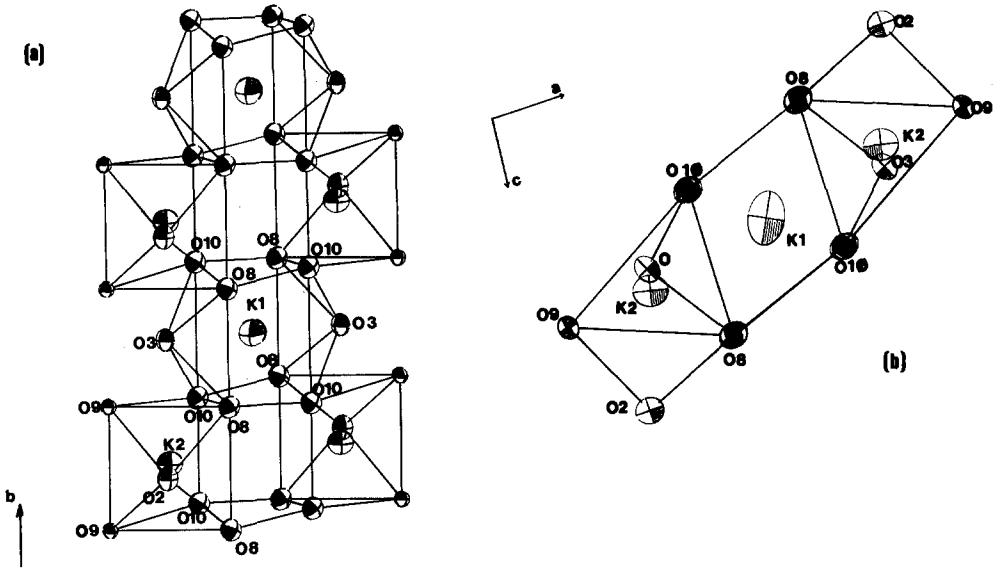

FIG. 5. (a) Three-dimensional view of an infinite chain of oxygen polyhedra about the K cations. (b) Projection along the *b* axis. The atoms are represented by their thermal ellipsoids. These chains link together the octahedral slabs and are not bridged laterally to adjacent chains.

the strength-to-length curve for the K–O bonds. The bicapped cubes around K(1) are comprised of two O(3), four O(8), and four O(10). The K(1)–O(8) distance is too large (3.304 Å) if the four O(8) are to be considered as first nearest neighbors. The large size of the K(1) sites is the result of the rigidity of the two-dimensional MoO_6-octahedron slabs. The large K(1)–O(8) separation is compensated by anomalously large thermal vibrations of K(1). The K(1) thermal ellipsoid has the major and intermediate axes in the plane formed by the four O(8). This can be interpreted as an indication that a large fraction of the K(1) thermal vibration is due to a distortion of the K(1) sublattice. Each K(1) cation is displaced along the major axis of the thermal ellipsoid in such a way as to be bonded to two O(8) only. At any given time the K(1) cations would have an 8-fold coordination rather than a 10-fold one.

(b) Thermal data and oxygen coordination. Although a quantitative analysis of the data reported in Table III will not be presented, qualitatively these data reveal many features of physical interest. For instance, the K cations have large and anisotropic thermal vibrations and K(1), which is more loosely bonded than K(2), has larger thermal vibrations than K(2). The large thermal ellipsoid of K(1) has been interpreted in the previous section. The major axis of the K(2) ellipsoid is directed away from any of the seven K(2)–O bonds. The thermal vibrations of the molybdenum cations are normal and only slightly anisotropic.

There are 11 crystallographically independent types of oxygen atoms. However, from the chemical bonding point of view there are only six types. Oxygens (1), (4), and (7) have similar bonding as each of them is bonded to two Mo atoms. Their thermal ellipsoids are quite anisotropic and in each case the major axis is perpendicular to the Mo–O–Mo bridges which link together the 10-octahedron units. Each of the oxygens, (2) and (3), forms one Mo–O bond and one K–O bond. Since for both oxygens

TABLE III

THERMAL DATA[a]

		$\bar{u}$	Angle/A	Angle/B	Angle/C
K(1)	1	0.269	129.6	90	34.8
Rb(1)		0.218	119.8	90	26.0
	2	0.162	90	0	90
		0.133	90	0	90
	3	0.138	39.6	90	55.2
		0.133	29.8	90	66.0
K(2)	1	0.169	35.6	90	59.2
Rb(2)		0.153	44.1	90	49.8
	2	0.147	90	0	90
		0.120	90	0	90
	3	0.129	125.6	90	30.8
		0.126	134.1	90	40.2
Mo(1)	1	0.101	75.7	90	19.0
		0.111	84.6	90	9.3
	2	0.089	90	0	90
		0.062	90	0	90
	3	0.082	14.3	90	109.0
		0.084	5.4	90	99.3
Mo(2)	1	0.098	50.6	93.2	44.3
		0.101	67.8	92.4	26.2
	2	0.085	77.4	14.1	97.3
		0.053	92.9	4.8	86.0
	3	0.077	42.1	103.7	133.4
		0.087	22.4	85.9	115.8
Mo(3)	1	0.106	45.1	82.2	50.7
		0.107	56.2	87.2	37.8
	2	0.084	100.9	10.9	89.1
		0.054	91.3	2.8	90.4
	3	0.075	133.0	97.6	39.4
		0.084	33.8	90.3	127.7
O(1)	1	0.163	68.7	70.2	33.4
		0.167	68.5	84.4	26.9
	2	0.108	106.4	22.0	102.7
		0.058	98.4	8.8	92.1
	3	0.081	27.4	81.0	120.3
		0.087	23.3	83.3	116.0
O(2)	1	0.150	90	0	90
		0.143	90	0	90
	2	0.132	28.0	90	66.7
		0.125	2.2	90	96.1
	3	0.114	118.0	90	23.3
		0.115	87.8	90	6.1
O(3)	1	0.138	59.7	90	35.1
		0.123	75.1	90	18.8
	2	0.138	90	0	90
		0.135	90	0	90
	3	0.084	30.3	90	125.1
		0.102	14.9	90	108.8
O(4)	1	0.130	71.9	90	22.8
		0.124	133.2	90	39.4
	2	0.114	18.1	90	112.8
		0.119	43.2	90	50.6
	3	0.088	90	0	90
		0.091	90	0	90
O(5)	1	0.130	84.6	90	10.1
		0.147	88.0	90	5.9
	2	0.095	90	0	90
		0.029	90	0	90
	3	0.087	5.4	90	100.1
		0.105	2.0	90	95.9
O(6)	1	0.109	110.8	90	16.0
		0.119	80.0	90	13.9
	2	0.101	20.8	90	74.0
		0.058	10.0	90	103.9
	3	0.082	90	0	90
		0.045	90	0	90
O(7)	1	0.157	50.6	90	44.2
		0.157	60.6	90	33.3
	2	0.096	39.4	90	134.2
		0.106	29.4	90	123.3
	3	0.093	90	0	90
		0.058	90	0	90
O(8)	1	0.144	36.0	124.6	102.6
		0.150	26.3	66.4	103.9
	2	0.134	60.1	36.9	111.9
		0.107	116.0	32.1	105.8
	3	0.110	71.9	78.8	25.6
		0.118	88.2	69.5	21.3
O(9)	1	0.112	68.6	96.4	27.0
		0.132	90.7	91.6	3.6
	2	0.095	74.4	15.6	90.7
		0.018	104.3	14.4	87.6
	3	0.083	27.0	104.2	117.0
		0.101	14.4	75.7	92.7
O(10)	1	0.144	42.2	130.5	103.5
		0.132	31.3	108.4	69.3
	2	0.131	48.4	41.8	90.5
		0.095	77.9	20.6	74.4
	3	0.107	84.4	98.6	13.5
		0.124	118.4	99.0	26.4
O(11)	1	0.116	77.0	19.1	77.4
		0.091	93.7	17.1	73.2
	2	0.098	51.4	109.1	49.1
		0.109	57.7	102.1	38.6
	3	0.086	41.6	90.6	136.3
		0.072	32.5	78.1	123.5

TABLE III—*Continued*

[a] For each position the first line gives the parameters of $K_{0.30}MoO_3$ while the second line gives those of $Rb_{0.30}MoO_3$.

the Mo–O bonds are rather short (about 1.69 Å), the minor axis of the thermal ellipsoid is directed along this bond. However, their anisotropy is somewhat different. This is probably due to the difference in length of the K–O bonds; K–O(2) = 2.703 Å is shorter than K–O(3) = 2.941 Å. The major axis of the O(2) ellipsoid is perpendicular to the shorter K(2)–O(2) bond. Both oxygens (5) and (6) are bonded to three Mo atoms, however, the respective thermal ellipsoids are slightly different, the former being more anisotropic than the latter. In both cases a short thermal vibration corresponds to the weak Mo(1)–O bond. This indicates that O(5) and O(6) are in between first- and second-nearest neighbors of Mo(1). Both oxygens (8) and (10) are surrounded by two cations, one Mo and one K. As can be seen from Table III, they have very similar thermal vibrations, slightly anisotropic with the ellipsoidal axes directed along the same directions within 10°. Oxygen (9) is bonded to three Mo and one K cations while O(11) is bonded to three Mo cations. Their thermal vibrations are normal and slightly anisotropic.

(c) Structural dimensionality. The structural dimensionality of a given compound depends upon which of its sublattices is taken into consideration. The physical properties also have the dimensionality of the sublattice which they are related to. In the case of $K_{0.30}MoO_3$, the K sublattice has the character of a one-dimensional lattice, the oxygen sublattice that of a three-dimensional lattice, and the Mo sublattice the character of an anisotropic two-dimensional lattice. In forming the slabs the 10-MoO_6-octahedron units share with the adjacent units eight octahedral corners along the *b* axis and four along the $[10\bar{1}]_I$ direction. The interatomic Mo–O distances corresponding to the Mo–O–Mo bonds across the shared corners, are about the same along both directions: Mo(2)–O(4) = 1.873 Å and Mo(3)–O(7) = 1.897 Å along the *b* axis and Mo(3)–O(1) = 1.890 Å along $[10\bar{1}]_I$.

Since there exist infinite chains of corner-sharing MoO_6 octahedra along the *b* axis, the mechanism of the electric conductivity along this axis is that of an ReO_3 or perovskite compound. It consists in electron transfers between Mo cations via Mo–O–Mo bonds. There also exist infinite chains of MoO_6 octahedra along the $[10\bar{1}]_I$ direction; however, along these chains the octahedra share sequentially three corners and one edge. Two mechanisms must be taken into account to explain the electric conductivity along the $[10\bar{1}]_I$ direction: that of the ReO_3 compounds for the corner-sharing octahedra and the mechanism of the rutile compounds for the edge-sharing octahedra. In the latter type of compounds the electron transfers take place between Mo cations across the shared edges. The different number of infinite chains of MoO_6 octahedra per unit cell along the *b* and $[10\bar{1}]$ directions (eight and four, respectively) and the different conduction mechanisms, explain qualitatively the anisotropy found for the electric conductivity by Brusetti *et al.* (*7*).

It is not possible to reconcile the structural dimensionality of $K_{0.30}MoO_3$ with the optical reflectivity measurements of Travaglini *et al.* (*8*). These authors found that at room temperature the optical reflectivity of $K_{0.30}MoO_3$ is that of a quasi-one-dimensional metallic compound. As stated above, in the structure of $K_{0.30}MoO_3$ only the K sublattice has a one-dimensional character. However, it is doubtful that the optical reflectivity is associated with the K sublattice.

(d) Charge distribution in the Mo sites. In compounds, such as $K_{0.30}MoO_3$, which contain the same element with more than one valence state, an important crystal chemical problem is to determine the distribution of Mo^{5+} and Mo^{6+} over the three crystallographically independent sites. This can be

done by analyzing the molybdenum–oxygen distances by the bond strength/bond length method (*16*). The strength of each individual Mo–O bond has been calculated by the use of the Zachariasen formula $D(s) = D(1)(1 - 0.166 \ln s)$, where $D(s)$ is the interatomic distance, s the bond strength, and $D(1)$ the interatomic distance for unit strength. The value of $D(1) = 1.890$ Å was given by Zachariasen for Mo–O (*16*). The individual values for the Mo–O bond strengths s are reported in Table II. The Mo valences have been obtained by summing the bond strengths over the anions surrounding each cation. The calculated average valence for the Mo sites is 5.732 which corresponds to a formula such as $K_{0.27}MoO_3$. At room temperature the charge distribution is

$$K^{+}_{5.36}[Mo(1)^{6+}_{0.880}Mo(1)^{5+}_{0.120}]_4 [Mo(2)^{6+}_{0.695}Mo(2)^{5+}_{0.305}]_8 [Mo(3)^{6+}_{0.694}Mo(3)^{5+}_{0.306}]_8O_{60}.$$

This distribution indicates that the site occupancy factor for the K cations is 89% and that 9, 45.5, and 45.5% of the Mo^{5+} are located in the (1), (2), and (3) Mo sites, respectively, namely 91% of the d electrons are equally distributed over those sites which contribute to the electric conductivity. As pointed out previously the least-squares structural refinement strongly indicated that the potassium sites are fully occupied. The two results can be reconciled by varying the $D(1)$ value in the Zachariasen formula. For instance, a value of $D(1)$ such as 1.888 Å would yield full occupancy for the potassium atoms while the distribution of the Mo^{5+} over the three Mo sites (1), (2), and (3) would remain approximatively the same (10, 45, and 45%, respectively). Therefore, we believe that the Zachariasen bond strength/bond length method, can give quite precisely the distribution of the 4*d* electrons over the Mo sites.

It must be pointed out that the cationic charge calculated for Mo(1) is larger than those calculated for Mo(2) and Mo(3), despite the fact that the values of the average interatomic distances for the three sites would seem to indicate the contrary. This erroneous correlation is due to the large distortion of the Mo(1) octahedron. This demonstrates the power of the Zachariasen method (*16*) for calculating cation valences of transition elements in oxide compounds.

(e) Lattice parameters versus temperature. In every curve of Fig. 3, except in that of the b parameter which varies smoothly down to 110 K, a discontinuity occurs at about 220 K. As can be seen from Fig. 2 of Ref. (*7*), the temperature of 220 K corresponds to the onset of the transition in the electric resistivity. It is clear from these curves that the thermal linear expansion coefficient, $\alpha = \Delta l/\Delta t \cdot l_{298}$, is strongly anisotropic. For instance, the thermal linear-expansion coefficient along the a direction is $\alpha_a \simeq 2.1 \times 10^{-5}$ K^{-1} and $\alpha'_a \simeq 1.3 \times 10^{-5}$ K^{-1} above and below the transition, respectively, while along the c direction the coefficient changes at the transition from $\alpha_c \simeq 3.1 \times 10^{-5}$ K^{-1} to $\alpha'_c \simeq 2.2 \times 10^{-5}$ K^{-1}. Since there is no discontinuity at the transition for the b parameter the coefficient $\alpha_b \simeq 0.07 \times 10^{-5}$ K^{-1} remains the same above and below the transition. Above the transition the value of α_b is smaller by a factor of 45 and 31 than the values α_c and α_a, respectively. Below the transition these factors become 30 and 18.5.

The thermal linear expansion anisotropy is better described by comparing the coefficients along the b direction, α_b, the $\mathbf{a}_I$–$\mathbf{c}_I$ vector, $\alpha_{\mathbf{a}-\mathbf{c}}$, and the d_{101} lattice spacing, α_{101}. These three directions are almost perpendicular to each other. The first two are contained in the octahedral slabs, while the third is almost perpendicular to them. Above the transition the coefficients are: $\alpha_b \simeq 0.07 \times 10^{-5}$ K^{-1}, $\alpha_{\mathbf{a}-\mathbf{c}} \simeq 1.07 \times 10^{-5}$ K^{-1}, and $\alpha_{101} \simeq 4.6 \times 10^{-5}$ K^{-1}. Below the transi-

tion the α_b coefficient remains the same whereas α_{a-c} and α_{101} become 0.35×10^{-5} and 3.3×10^{-5} K^{-1}, respectively. These results confirm that the octahedral slabs form a rigid system, especially along the *b* axis. By decreasing the temperature the structure contracts mainly along the direction perpendicular to the octahedral slabs and consequently the K–O bonds become stronger.

As pointed out above, the K polyhedra are linked to the octahedral slabs only via corner sharing, therefore the structure can "breathe" around the potassium polyhedra. One can surmise that at the transition the structural rearrangement takes place mainly around the K atoms. In order to reestablish the electrostatic balance, the oxygen and the molybdenum atoms would also move, the *d* electrons would transfer from one site to another and the Mo–Mo pairs would form throughout the structure. These pairs are needed if the phase transition occurring in $K_{0.30}MoO_3$ at 180 K is of Peierls type as suggested by Travaglini *et al.* (*8*). Another possible model would be that at the transition the *d* electrons transfer to the Mo(1) sites which, being isolated, could not contribute to the electrical conductivity. In this case there would not be any pair formation. A structural determination of the insulating phase should reveal the correct model.

(2) $Rb_{0.30}MoO_3$

As can be seen from Table I–III the structure of $Rb_{0.30}MoO_3$ is very similar to that of $K_{0.30}MoO_3$. The average Mo–O distances in $Rb_{0.30}MoO_3$ are somewhat larger than the corresponding ones in the K counterpart, but the sequence of the three distances is exactly the same: Mo(1)–O is larger than Mo(2)–O and Mo(3)–O, which are about equal. In a few cases the individual Mo–O distances varied appreciably and these variations led to a slightly different charge distribution for the Mo cations. The rubidium polyhedra exhibit exactly the same features as their potassium counterparts. As expected the Rb polyhedra are larger, but the ratio of the average distances, d_{Rb-O}/d_{K-O}, is smaller for both sites than the ratio of the ionic radii. For example, the average-distance ratio for sites (1) and (2) is 1.018 and 1.026, respectively, while that of the ionic radii is 1.05. This indicates that the Rb–O bonds are relatively shorter and thus stronger than the K–O bonds and that the size effect is in part compensated by stronger bonds.

The thermal vibrations of the rubidium atoms are very similar to those of the potassium atoms in $K_{0.30}MoO_3$. The angles, which give the principal axis orientation of the thermal ellipsoids with respect to the crystallographic axes, differ by less than 10°. A small, but significant difference exists in the length of the major axis for site (1); that of Rb(1) is shorter than the major axis of K(1). This is due to the larger size of the Rb cations. If one accepts the model that the large vibrations of K(1) and Rb(1) are due to the distortions of the alkali cation lattice, smaller Rb(1) displacements toward two of the four O(8), are needed in order to obtain the same bond strength and consequently the electrostatic balance. The thermal vibrations of the Mo atoms in $Rb_{0.30}MoO_3$ are much more anisotropic than in $K_{0.30}MoO_3$. For the three sites the short axes are nearly equal and directed along the *b* axis. The thermal ellipsoids of Mo(2) and Mo(3) have no constraints due to the point symmetry and yet in each case the minor axis is within less than 4° from the *b* axis. The oxygen atoms have a large thermal anisotropy. In particular, O(5), O(7), and O(9) exhibit anomalously small vibrations along the *b* axis. These atoms have the same coordination with respect to the Mo cations, namely each is coordinated to three Mo cations. However, we cannot find any crystal chemical argument to explain this unique behavior.

The calculations of the cation charges by the Zachariasen method (*16*) gives the following valence distribution for the Mo cations:

$$[Mo(1)^{6+}_{0.730}Mo(1)^{5+}_{0.270}]_4$$
$$[Mo(2)^{6+}_{0.635}Mo(2)^{5+}_{0.365}]_8$$
$$[Mo(3)^{6+}_{0.635}Mo(3)^{5+}_{0.365}]_8.$$

Qualitatively this charge distribution agrees well with that found in $K_{0.30}MoO_3$. The (1) sites contain much less Mo^{5+} (16% of the total Mo^{5+} cations) than the other two sites. The remaining 4*d* electrons are equally distributed over the (2) and (3) sites (42% in each). These values are to be compared with 10, 45, and 45% for the (1), (2), and (3) sites in $K_{0.30}MoO_3$, respectively. The significant difference between the two bronzes is in the sites (1) occupancy; those of $Rb_{0.30}MoO_3$ contain more 4*d* electrons than the corresponding sites of $K_{0.30}MoO_3$. However, the difference could be due to the lower precision in the interatomic distances, obtained in the structural refinement of $Rb_{0.30}MoO_3$. For example, the Zachariasen formula applied to $Rb_{0.30}MoO_3$ yielded an unreal number of Rb atoms per unit cell, namely 6.92 instead of 6, which represents the maximum of alkali cations in a unit cell. The value of $D(1)$ calculated for 6.00 Rb atoms per cell unit cell is 1.892 Å, as against 1.890 Å proposed by Zachariasen and 1.888 Å found for $K_{0.30}MoO_3$. The value of 1.892 Å yields 14, 43, and 43% for the 4*d* electron distribution over the three Mo sites. This indicates again that the Zachariasen method can give quite reliably the charge distribution of the Mo^{5+} and Mo^{6+} cations but not the occupancy factor of the alkali metals.

Acknowledgments

The authors thank J. Mercier and C. Schlenker for valuable discussions.

References

1. A. Wold, W. Kunnmann, R. J. Arnott, and A. Ferretti, *Inorg. Chem.* **3,** 545 (1964).
2. N. C. Stephenson and A. D. Wadsley, *Acta Crystallogr.* **18,** 241 (1965).
3. J. Graham and A. D. Wadsley, *Acta Crystallogr.* **20,** 93 (1966).
4. G. H. Bouchard, Jr., J. H. Perlstein, and M. J. Sienko, *Inorg. Chem.* **6,** 1682 (1967).
5. D. S. Perloff, M. Vlasse, and A. Wold, *J. Phys. Chem. Solids* **30,** 1071 (1969).
6. W. Fogle and J. H. Perlstein, *Phys. Rev. B* **6,** 1402 (1972).
7. R. Brusetti, B. K. Chakraverty, J. Devenyi, J. Dumas, J. Marcus, and C. Schlenker, *Recent Dev. Condensed Matter Phys.* **2,** 181 (1981).
8. G. Travaglini, P. Watcher, J. Marcus, and C. Schlenker, *Solid State Commun.* **37,** 599 (1981).
9. G. Travaglini, I. Mönke, and P. Wachter, *Solid State Commun.* **45,** 289 (1983).
10. J. Dumas, C. Schlenker, J. Marcus, and R. Buder, *Phys. Rev. Lett.* **50,** 757, 1983.
11. J. P. Pouget, S. Kagoshima, C. Schlenker, and J. Marcus, *J. Phys. (Paris) Lett.* **44,** L113 (1983).
12. C. H. Chen, L. F. Schneemeyer, and R. M. Fleming, *Phys. Rev. B* **29,** 3765 (1984).
13. R. M. Fleming and L. F. Schneemeyer, *Bull. Amer. Phys. Soc.* **29,** 470 (1984).
14. S. B. Dierker, K. B. Lyons, and L. F. Scheemeyer, *Bull. Amer. Phys. Soc.* **29,** 469 (1984).
15. P. Strobel and M. Greenblatt, *J. Solid State Chem.* **36,** 331 (1981).
16. W. H. Zachariasen, *J. Less-Common Met.* **62,** 1 (1978).
17. H. Vincent, M. Ghedira, J. Marcus, J. Mercier, and C. Schlenker, *J. Solid Chem.* **47,** 113 (1983).